Constraining the sedimentology and stratigraphy of submarine intraslope lobe deposits using exhumed examples from the Karoo Basin, South Africa

Y.T. Spychala[1]*, D.M. Hodgson[1], S.S. Flint[2], N.P. Mountney[1]

[1]Stratigraphy Group, School of Earth and Environment, University of Leeds, LS2 9JT, UK

[2] Stratigraphy Group, School of Earth, Atmospheric and Environmental Science, University of Manchester, M13 9PL, UK

*Corresponding author: Yvonne T. Spychala; eeyts@leeds.ac.uk ; phone: 44 (0)113 343 0236

Co-authors emails: d.hodgson@leeds.ac.uk; stephen.flint@manchester.ac.uk; n.p.mountney@leeds.ac.uk

Abstract

Intraslope lobe deposits provide a record of the infill of accommodation on submarine slopes and their recognition enables the accurate reconstruction of the stratigraphic evolution of submarine slope systems. Extensive exposures of discrete sand-prone packages in Units D/E and E, Fort Brown Formation, Karoo Basin, South Africa, permit analysis of the sedimentology and stacking patterns of three intraslope lobe complexes and their palaeogeographic reconstruction via bed-scale analysis and physical correlation of key stratal surfaces. The sand-prone packages comprise tabular, aggradationally to slightly compensationally

stacked lobe deposits with constituent facies associations that can be attributed to lobe axis, lobe off-axis, lobe-fringe and distal lobe-fringe environments. Locally, intraslope lobe deposits are incised by low aspect ratio channels that mark basinward progradation of the deepwater system. The origin of accommodation on the slope for lobe deposition is interpreted to be due to differential compaction or healing of scars from mass wasting processes. The stacking patterns and sedimentary facies arrangement identified in this study are distinct from those of more commonly recognised basin-floor lobe deposits, thereby enabling the establishment of recognition criteria for intraslope lobe deposits in other less well exposed and studied fine-grained systems. Compared to basin floor lobes, intraslope lobes are smaller volume, influenced by higher degrees of confinement, and tend to show aggradational stacking patterns.

Keywords

intraslope lobes; submarine slope; slope topography; facies stacking pattern; facies variability; Karoo Basin

1. Introduction

Basin floor lobe deposits are the dominant component of submarine fan successions and criteria for their recognition are well established (e.g., Harms, 1974; Hartog Jager et al., 1993; Sixsmith et al., 2004; Pyles, 2008; Prélat et al., 2009, 2010; Pyles and Jenette, 2009; Kilhams et al., 2012; Etienne et al., 2012; Burgreen and Graham,

2014). By contrast, the characteristics of intraslope lobes, which are also referred to as perched lobes (Plink-Björklund and Steel, 2002; Prather et al., 2012a) or transient fans (Adeogba et al., 2005; Gamberi and Rovere, 2011), which form in areas of slope accommodation, are poorly defined (Fig. 1). Intraslope lobes have been identified in several subsurface geophysical studies based on multibeam bathymetric data, CHIRP profiles and seismic imaging (2D and 3D). Documented examples include studies from the Gulf of Mexico (Prather et al., 1998; Fiduk et al., 1999; Pirmez et al., 2012; Prather et al., 2012b), the Niger Delta continental slope offshore Nigeria (Adeogba et al., 2005; Li et al., 2010; Barton, 2012; Prather et al., 2012a), the Lower Congo Basin, offshore Angola (Oluboyo et al., 2014), the Algarve Margin, offshore Portugal (Marchès et al., 2010), the Gioia Basin, southeastern Tyrrhenian Sea (Gamberi and Rovere, 2011; Gamberi et al., 2011) and the Baiyun Sag, South China Sea (Li et al., 2012).

The geophysical expression of intraslope lobes is described as layered (high amplitude reflectors) to transparent seismic facies by most authors (Booth et al., 2003; Adeogba et al., 2005; Li et al., 2012), though Marchès et al. (2010) report cases that are represented by chaotic seismic reflectors. These seismic facies have been interpreted as channel-lobe systems and associated mass transport deposits, respectively. Different mechanisms are invoked to explain the development of intraslope accommodation needed for intraslope lobe deposits to form, including tectonics (Marchès et al., 2010; Li et al., 2012), mud diapirism (Adeogba et al., 2005),

74 halokinesis (Booth et al., 2003; Oluboyo et al., 2014) or slide scars
75 (Morris et al., 2014a). Several commonly observed features of
76 intraslope lobes are considered as diagnostic indicators: 1) a smaller
77 lateral extent and lower aspect ratio than basin floor lobes (Plink-
78 Björklund and Steel, 2002; Deptuck et al., 2008); 2) common
79 evidence for incision due to their transience that is linked to a lower
80 base level on the basin floor (Adeogba et al., 2005; Flint et al., 2011;
81 Barton, 2012; Prather et al., 2012b) or to slope profiles that are not
82 in equilibrium (Ferry et al., 2005); 3) association with mass transport
83 complexes (MTCs) (Adeogba et al., 2005; Gamberi and Rovere, 2011;
84 Li et al., 2012); 4) deposits delimited by onlap and downlap
85 terminations (Booth et al., 2003; Li et al., 2012); 5) prevalence of
86 coarse sand sediment that is deposited in response to hydraulic
87 jumps due to a break-in-slope related to a stepped slope profile
88 (Komar, 1971; Ferry et al., 2005); and 6) mounded or tabular
89 morphologies (e.g., Oluboyo et al., 2014).

90 Intraslope lobes are important features in the reconstruction of the
91 evolution of the slope and the analysis of sediment dispersal
92 patterns, and indicate the presence of an uneven slope profile
93 during deposition. Although attempts have been made to determine
94 the importance of submarine slope deposits within a source-to-sink
95 system (Eschard et al., 2004), intraslope lobes have rarely been
96 identified in outcrop studies (Plink-Björklund and Steel, 2002;
97 Sinclair and Tomasso, 2002; Beaubouef et al., 2007; Figueiredo et
98 al., 2010; Bernhardt et al., 2012; van der Merwe et al., 2014).
99 Therefore, the sub-seismic depositional architecture of intraslope

lobes can be considered as one of the missing pieces in understanding the stratigraphic record of deep-marine systems and their preserved successions.

Extensive fieldwork carried out in the Laingsburg depocentre of the Karoo Basin, South Africa (e.g., Grecula et al., 2003a; Sixsmith et al., 2004; Di Celma et al., 2011; Flint et al., 2011; Hodgson et al., 2011; Brunt et al., 2013a; Morris et al., 2014b; van der Merwe et al., 2014), has established the stratigraphic and palaeogeographic framework in detail and enables the identification of lobes that were deposited in a slope setting. In this study, we focus on a more detailed characterisation of some of the intraslope lobes of the Karoo Basin. Specific objectives are: 1) to determine the characteristic facies associations and anatomies of the intraslope lobes in the study area; 2) to compare their characteristics with those of basin floor lobes; and 3) to discuss the origin of the transient slope accommodation. The establishment of recognition criteria for the identification of intraslope lobes will help reduce uncertainties in the interpretation of depositional environments observed in core and outcrop where the palaeogeographic context is not clear.

2. Geological and Stratigraphic Settings

123 The evolution of the Karoo Basin has long been associated with a
124 magmatic arc and the tectonics of a fold-thrust belt (Cape Fold Belt;
125 Fig. 2a), thus characterising it as a retroarc foreland basin (Visser
126 and Prackelt, 1996; Visser, 1997; Catuneanu et al., 1998). Recent
127 studies (e.g., Tankard et al., 2009) suggest that an early phase of
128 subsidence enabled a basin fill that pre-dates the initiation of the
129 Cape Orogeny, and was induced by dynamic topography. This
130 topography is thought to have been derived from the coupling of
131 mantle flow processes to distant subduction of the palaeo-Pacific
132 Plate (Pysklywec and Mitrovica, 1999).

133 The Laingsburg depocentre is located in the south-western part of
134 the Karoo Basin and adjacent to the present-day Cape Fold Belt
135 (Flint et al., 2011). The stratigraphic unit of study is the Fort Brown
136 Formation of the Ecca Group, which is exposed along the limbs of
137 large, post-depositional folds (Fig. 2b). The Fort Brown Formation is
138 a 400 m-thick submarine slope succession (Di Celma et al., 2011;
139 Flint et al., 2011; Hodgson et al., 2011) that overlies the Laingsburg
140 Formation, a 550 m-thick sand-rich basin floor and base-of-slope
141 succession (Sixsmith, 2000; Grecula et al., 2003a, 2003b; Sixsmith et
142 al., 2004; Brunt et al., 2013b). The Fort Brown Formation is divided
143 into Units C to G (Flint et al., 2011; van der Merwe et al., 2014).
144 These sand prone-units are each separated by regional hemipelagic
145 claystones that locally include additional thin (1-15 m-thick)
146 intercalated sand-prone units informally referred to as interfans
147 (B/C interfan and D/E interfan) (Grecula, 2003a; Hodgson et al.,
148 2011). The sequence stratigraphy of the Fort Brown Formation has

been proposed by Flint et al. (2011) to comprise two composite sequence sets, the lower one containing units B/C, C and D and the upper one containing units D/E, E and F. Each individual unit represents a lowstand sequence set, with subunits. For example Unit E is divided into Subunits E1, E2, and E3 based on the occurrence of claystone layers of regional mapped extent. Each subunit is interpreted as a lowstand systems tract. In this framework, the regional claystones that separate the units are interpreted as associated transgressive (TST) and highstand (HST) sequence sets and the equally widespread claystones between sub-units are interpreted as combined transgressive and highstand systems tracts that record the deep-water expression of maximum flooding surfaces (Flint et al., 2011). Limited chronostratigraphic age control in the Fort Brown Formation (McKay et al. 2015) precludes establishment of the duration of depositional sequences.

This study focuses on two areas. Exposures of the Unit D/E interfan and Subunit E1 in the NW area of Zoutkloof (Fig. 2b) have been interpreted previously as lobes that formed in a slope setting (Figueiredo et al., 2010), but have not been hitherto characterised in detail. Four correlation panels were constructed (Zoutkloof S, Zoutkloof N, Roggekraal and Roggekraal N) to illustrate down-dip and strike variations in the successions. Unit E2 in the Geelbek area (Fig. 2b) comprises tabular sand-rich deposits, which, based on a detailed regional dataset, are interpreted to be intraslope lobes that formed above a stepped slope profile up-dip of a ramp dominated by sediment bypass (van der Merwe at al., 2014). The existence of

these intraslope lobe deposits demonstrates the location and timing of slope accommodation and can be used to constrain the stratigraphic evolution of the Laingsburg submarine slope system.

3. Methodology and Dataset

For this study, 125 measured sections (each ranging from 3 to 36 m in length and totalling 2.8 km in cumulative thickness) were logged at 1:50 scale in the field, recording grain size, sedimentary structures and the nature and extent of bounding surfaces. In the Zoutkloof area (Fig. 2b,d), 80 sedimentary logs and 422 palaeocurrent measurements from ripple lamination and climbing-ripple lamination were collected over three large, adjacent fold limbs to reconstruct the large-scale geometries of exhumed intraslope complexes (Fig. 2b). In the south-eastern study area (Geelbek area; Fig. 2b,e), 45 sedimentary logs and 173 palaeoflow measurements were collected from ripple lamination, climbing ripple lamination and tool marks along an oblique dip section. In areas of specific interest, 11 additional detailed short sections were measured and correlated (Fig. 2e). This has permitted the development of a detailed sedimentological model to account for facies distributions and small-scale geometries. Correlation panels for the Geelbek area are hung from the regional claystones separating subunits E2 and E3. The Zoutkloof correlation panels are hung from the base of Unit D/E that overlies a regional claystone above Unit D.

4. Facies associations

Six facies associations (FA) are identified based on inferred sedimentary processes and depositional environment. Five of the six facies associations represent particular lobe sub-environments (lobe axis, lobe off-axis, lobe fringe and distal lobe fringe) and have been modified from Prélat et al. (2009) according to the observed facies in the intraslope lobe deposits. FA1-5 represent lobe axis to lobe distal fringe, whereas FA 6 represents hemipelagic background sedimentation.

4.1 FA 1: Thick-bedded sandstone

Observations. This facies association is dominated by structureless, 0.7 to 2.5 m-thick beds of lower to upper fine-grained sandstone that commonly contain parallel lamination with some lenticular mudstone chips (mm-sized) aligned parallel to the laminae. Overall, beds are moderately to well sorted. Most beds lack grading, though weak normal grading is observed towards the tops of some beds that consist of 2 to 10 cm-thick caps of mica-rich, moderately sorted silty sandstone. Intraformational mudclasts are rarely observed at bed bases. Bed bases are sharp, loaded or erosive and can preserve tool marks. Bed amalgamation is common and can lead to > 10 m-thick packages of structureless sandstones (high-amalgamation zones; Fig. 3a). Amalgamation surfaces are indicated by discontinuous layers of mudclasts or subtle grain size breaks.

Amalgamated sandstone packages can overlie surfaces that truncate underlying strata by up to 5 m. These surfaces are mantled with thin layers of mudstone clast conglomerates. Thick-bedded sandstones show tabular geometries. They are laterally extensive for up to 6 kms.

Interpretation. Thick-bedded, structureless and amalgamated sandstones with weak normal grading are interpreted to be the deposits of high-density turbidity currents (Kneller and Branney, 1995) with high aggradation rates (Arnott and Hand, 1989; Leclair and Arnott, 2005; Talling et al., 2012). Their geometries, thickness and facies conform to lobe- or channel-axis settings (e.g., Prélat et al., 2009; Brunt el al., 2013a).

4.2 FA 2: Medium- to thin-bedded structured sandstone

Observations. This facies association comprises lower fine- to very-fine-grained, normally graded sandstone beds that are well sorted. Bed thicknesses range from 0.1 to 0.7 m. Sedimentary structures present include planar lamination, wavy lamination, current-ripple lamination and climbing-ripple lamination (Fig. 3b). Climbing-ripple lamination can be observed with supercritical angles of climb whereby stoss sides are preserved. The majority of beds contain two or more of these sedimentary structures. A common pattern is the vertical repetition of climbing-ripple laminations that are transitional to wavy laminations. Ripple foresets can be draped by

thin (<0.1 cm thick) silty laminae. Individual beds can preserve multiple flow directions. Carbonaceous material and mud chips are dispersed in the sandy matrix. Bed bases are sharp or loaded. Medium- to thin-bedded sandstones show tabular geometries and can be traced for kms down-dip and in strike section.

Interpretation. This facies association is interpreted to be deposited by low-density turbidity currents in a lobe off-axis setting. Bedforms such as planar lamination and current-ripple lamination are produced beneath dilute turbulent flows, which rework sediment along the bed (Allen, 1982; Southard, 1991; Best and Bridge, 1992). Beds with opposing palaeocurrent indicators suggest reflection and deflection of the flow (Edwards et al., 1994). Beds with repeating patterns of climbing-ripple and wavy lamination are interpreted to indicate highly unsteady flow behaviour due to either long-lived surging or collapsing flows (Jobe, 2012).

4.3 FA 3: Interbedded thin-bedded sandstones and siltstones

Observations. This facies association comprises thin-bedded (0.01 to 0.2 m), very-fine-grained sandstone interbedded with sandy siltstone and coarse to fine siltstone. Sandstone beds show planar, current-ripple or wavy lamination, whereas siltstone beds commonly display planar lamination with rare isolated starved ripple forms at their base where there is a sand component to the siltstone (Fig. 3c). Contacts between sandstone and siltstone beds

are sharp, undulating or loaded. Stoss-side preservation of climbing ripple lamination in sandstone beds is observed in 2D, and ripple geometries are locally preserved as sigmoid-shaped bedforms where 3D observations are possible (see Fig. 12b in Kane and Hodgson, 2011,). Commonly, interbedded sandstones and siltstones form stacked, aggradational packages up to 5 m thick, which internally show no discernible trends in grain size or bed thickness. Individual packages dominantly comprise ripple and climbing-ripple laminated sandstones in their lower part and planar laminated sandstones in their upper part.

Interpretation. Ripple lamination formed due to reworking by dilute turbulent flows with moderate aggradation rates, whereas climbing-ripple lamination is indicative of high aggradation rates (Allen, 1971; Allen, 1982; Southard, 1991). Ripple and planar laminated packages correspond with T_C and T_D divisions of Bouma (1962). This facies association is interpreted as a combination of deposition from sluggish, small-volume flows (Jobe et al., 2012) and flows that underwent rapid deceleration that led to high rates of sediment fallout. This implies that some flows were responding to changes in confinement, similar to flows that undergo expansion and rapid deposition when exiting channel confinement (e.g., Morris et al., 2014b). Observed facies and thicknesses of this facies association conform to an interpretation of a lobe-fringe setting.

4.4 FA 4: Bipartite beds

Observations. Bipartite sand-prone beds (0.01 to 1.5 m thick) are composed of a lower and upper division. The well sorted lower division that comprises relatively clean, structureless sandstone with low mud content. The upper division comprises poorly sorted mica-rich argillaceous sandstone that contains sand grains that are coarser than in the lower division, and varied proportions of subangular to subrounded mudstone clasts (mm to cm sized), mudstone chips and carbonaceous material (plant fragments) (Fig. 3d). Mudstone clasts show no preferred orientation. Typically, the boundary between the lower and upper divisions is gradational. Bed bases are sharp, whereas bed tops can be undulose.

Interpretation. Bipartite beds are interpreted to be the result of a juxtaposition of a high-density turbidity current and a genetically linked cohesive debris flow - a type of hybrid bed (Haughton et al., 2009). Several authors have identified an increase in the number of turbidites with linked debrites in distal parts of basin floor lobes (e.g., Ito, 2008; Hodgson et al., 2009; Talling et al., 2012; Grundvåg et al., 2014). Therefore, bipartite beds are interpreted to be deposited in lobe-fringe settings.

4.5 FA 5: Thin- bedded siltstone

Observations. Thin-bedded (sandy), fine- to coarse-grained siltstones (0.05 to 0.1 m) form metre-scale packages with rare thin (>0.05 m), very fine-grained sandstones that are well sorted (Fig.

3e). Typically, beds are structureless or planar laminated and some incorporate mudstone chips (up to 20% of the bulk volume). Some sandy siltstone beds show isolated starved ripple forms at their base. Thin-bedded siltstones can show minor bioturbation.

Interpretation. Siltstone deposits are interpreted as the preserved products of dilute turbidity currents in distal lobe-fringe settings. Structureless beds are attributed to direct suspension fallout (Bouma, 1962), whereas planar laminated beds are produced by traction (Stow and Piper, 1984; Mutti, 1992; Talling et al., 2012).

4.6 FA 6: Regional claystone

Observations. Homogenous intervals of (silty) claystone (Fig. 3f) are up to 22 m thick. Layers of concretions are common and tend to be associated with distinct horizons in the deposits. Claystone intervals are laterally extensive for tens of kilometres, except where eroded by channelised flows. Thin (<10 cm) ash layers and thin-bedded (mm-scale) graded siltstone units are locally intercalated with the claystones.

Interpretation. Claystones are interpreted as hemipelagic background deposits. Where mapped over large areas, they mark episodes of sediment starvation to the deep basin, and are interpreted to contain the deep-water expression of maximum flooding surfaces (e.g., Flint et al., 2011). Such packages therefore serve as useful correlation intervals.

5. Architecture

Unit D/E and Subunits E1 and E2 of the Fort Brown Formation have been recognized as tabular, sand-prone units within the submarine slope succession (Grecula et al., 2003b; Figueiredo et al., 2010). Flint et al. (2011) placed these packages into the overall sequence stratigraphic framework and van der Merwe et al. (2014) confirmed their palaeogeographic position on the slope. For the first time, the distribution of architectural elements and facies associations of these units are presented and discussed.

The identification of architectural elements is based on cross-sectional geometry, spatial extent, distribution of sedimentary facies and bounding surfaces marked by abrupt changes in facies (Fig. 4). Interpreted architectural elements include lobe deposits, channel-fills and drapes (Fig. 4).

5.1 Zoutkloof area

Unit D/E. Unit D/E is a tabular sandstone package, informally referred to as an interfan (Flint et al., 2011), with a basal interval of interbedded siltstones and very fine-grained sandstones and a sharp top (Fig. 4a). The spatial extent of Unit D/E is limited to the Zoutkloof and Roggekraal study area (81 km^2; Figueiredo et al., 2010). Overall, palaeocurrent direction is to the ENE, but climbing ripple-laminated sandstones at Zoutkloof S show some readings to the west (Figs. 5, 6). Unit D/E is thickest (10 m) in the Zoutkloof N

and Roggekraal areas where it comprises amalgamated thick-bedded structureless sandstones (FA 1) (Fig. 5). Across strike to the south (Zoutkloof S), a 6 m heterolithic package (FA 3) sharply overlies very fine- and fine-grained structured sandstones (FA 2). Unit D/E is not observed 6 km along strike to the south, which constrains the southward (lateral) pinch-out (Fig. 6). Across strike to the north (Roggekraal North; Fig. 4b), a 7 m-thick succession of structured sandstone (FA 2) is sharply overlain by structureless sandstones (FA 1).

Interpretation. Overall, the axis of Unit D/E is in the Zoutkloof N and Roggekraal areas, with more off-axis and fringe deposits in the south and north. The stratigraphic changes in facies in the Zoutkloof S and Roggekraal N areas suggest that Unit D/E comprises at least two lobes, and therefore represents a lobe complex (*sensu* Prélat et al., 2009). The lower lobe extends further south than the upper lobe, with lobe off-axis deposits (FA 2) overlain by lobe-fringe deposits (FA 3) in Zoutkloof S and lobe off-axis deposits (FA 2) overlain by lobe-axis deposits (FA 1) in Roggekraal N (Fig. 5) suggesting a minor compensational stacking pattern. The lobe axes are amalgamated in the central part of the study area.

The westward palaeocurrents in deposits in Zoutkloof S are interpreted to indicate rapid deposition of turbidity currents deflected and reflected off seabed topography at the fringes of the intraslope lobe (Fig. 6). There is no evidence of incision into the Unit D/E deposits and no deposit of this age directly down-dip has been

recognized (van der Merwe et al., 2014). The abandonment of Unit D/E suggests that either the sediment routing system avulsed outside of the study area or sand-grade sediment supply ceased prior to the complete infill of the slope accommodation.

Subunit E1. E1 is separated from Unit D/E by a 10 m thick mudstone, and has a basal ~0.5 m-thick interval of interbedded mudstone, siltstone and very fine-grained sandstone. The dominant palaeoflow is to the E, which is consistent with regional trends, whereas some deposits show palaeoflow to the W in the Zoutkloof S area (Figs. 5, 6). Where thickest (14 m), E1 is characterised by structureless amalgamated sandstones (FA 1) and structured sandstones (FA 2). In Roggekraal N, to the north where E1 is 8 m-thick, 3 packages are identified by sharp contacts with thin-bedded siltstones (FA 5) units. The lowermost unit is dominated by heterolithic deposits (FA 3), the middle is dominated by FA 1, and the upper is dominated by FA 2 (Fig. 4b). In contrast, to the south at Zoutkloof S, E1 is thinner (5 m) and comprises heterolithic packages (FA 3) and thin-bedded siltstones (FA 5). E1 is not observed 6 km along strike to the south, which constrains the southward (lateral) pinch-out (Fig. 6). Locally, E1 is truncated by erosion surfaces from multiple stratigraphic levels (Figueiredo et al., 2010, 2013;) (E1, E2, E3 and Unit F;, Fig. 6). Erosion surfaces within E1 cut down up to 10 m and are overlain by thick-bedded sandstones that have low aspect ratios (10:1 to 15:1;

Fig. 4). Younger erosion surface commonly have higher aspect ratios (20: 1 to 35: 1; Fig. 5) and are overlain by thin bedded, and locally tightly folded, sandstones and siltstones (Figueiredo et al., 2010, 2013), but sand-filled younger channel-fills are also observed.

Interpretation. In Roggekraal N, thin siltstone packages that abruptly separate three axis and off-axis packages indicate the existence of three lobes in the lobe complex (Fig. 4). The distribution of the lobe axis and off-axis deposits, and the lobe fringe and distal fringe deposits of the individual lobes, suggest an aggradational to slightly compensational stacking pattern. Deviation from the regional palaeocurrent trend in Zoutkloof S is interpreted to indicate deflection and reflection of turbidity currents off seabed topography. Erosion surfaces overlain by sandstones are interpreted as W-E and NW-SE oriented channel-fills.

5.2 Geelbek area

Subunit E2. Subunit E2 comprises three packages based on thickness trends, facies distribution, bounding surfaces and palaeocurrents measurements (Figs. 7a-d, 8). The mean palaeocurrent direction is to the E, but with local variations (Fig. 8). The base of the lower package, E2A, consists of heterolithic deposits (FA 3) overlain by FA 1 and FA 2 beds with abundant dm-scale erosion surfaces (Fig. 9a). Commonly, medium-bedded, structured sandstones (FA 2) display

443 more than one sedimentary structure vertically and laterally (planar
444 lamination, ripple lamination and climbing-ripple lamination).
445 Lateral facies transitions in individual beds include ripple-, through
446 wavy-, to planar-lamination, which occur over tenss of metres
447 lateral extent.

448 In some beds, palaeocurrent measurements from stoss-side
449 preserved climbing ripple-lamination can display ENE palaeocurrents
450 in the lower section whereas the upper section preserves
451 palaeocurrents to the WSW (e.g., Marker bed 1 (Mb1), see Fig. 7-
452 9a). Typically, these beds are thickest in the east and thin westward
453 in an up-dip direction. Sedimentary structures change in the
454 direction of thinning from stoss-side preserved climbing-ripple
455 lamination, through planar lamination with isolated current-ripple
456 forms, to planar laminated sandstones. The bases of some beds with
457 bi-directional palaeocurrents (e.g., Marker bed 2 (Mb2), see Fig. 9a)
458 truncate underlying bedding with siltstones that display soft-
459 sediment deformation structures (Fig. 7b).

460 The middle package, E2B, is defined by a stepped basal erosion
461 surface that incises 6 m into E2A (Fig. 8). The overlying sediments
462 comprise highly amalgamated thick-bedded sandstones (FA 1) with
463 rare planar lamination on bed tops (Fig. 8). These pass into more
464 clearly stratified but internally structureless fine-grained sandstones
465 close to the (oblique) margin of the cut and can be traced out for
466 over a km away beyond the basal scour surface, where E2B overlies

467 E2A concordantly (Fig. 7c). Palaeocurrents from grooves indicate an
468 overall ENE-WSW flow direction (Fig. 8).

469 The upper E2C division is the most laterally extensive of Subunit E2
470 and the boundary with E2B is marked by a thin siltstone horizon
471 (~10 cm; FA 5; Fig. 7d). It comprises basal bipartite beds (FA 4) in its
472 proximal (westerly) section and is largely made up of medium-
473 bedded, structured sandstones (FA 2) that overlie the highly
474 amalgamated sandstones of E2B (FA 1). Thin-bedded deposits (FA 3
475 and FA 5) are rare. Palaeocurrents measured from current- and
476 climbing-ripple lamination indicates an easterly flow direction (Fig.
477 8). In the west, beds are structureless (FA 1), with rare ripple
478 lamination showing easterly palaeocurrents. Structureless
479 sandstone beds onlap westward onto the underlying claystone,
480 overstepping the E2A and B deposits (Fig. 8). Commonly, the
481 onlapping beds show pinching and swelling close to the onlap
482 surface as well as evidence of erosion (rip-up clasts, truncation).
483 Clastic injectites are abundant in the mudstone that underlies the
484 sandstone onlap (Fig. 9b).

485 In the underlying claystone that separates Units D and E, a
486 distinctive 0.4 m-thick intraformational clast-rich bed is used as a
487 local marker bed. The sandstone bed and bounding claystones are
488 present in western part of the outcrop. However, they terminate
489 abruptly eastward against a steep surface overlain by a thin-bedded
490 coarse siltstone and silty claystone succession below where the
491 overlying E2 attains its maximum thickness (Fig. 8). The thin-bedded

siltstone unit forms a discrete ~30 m-thick unit that thins out over ~700 m to the east; by contrast, the western edge is steep and abrupt (Fig. 8).

Interpretation. The high sand-content and tabular geometry, the underlying and overlying channel-levee systems (e.g., Brunt et al 2013b), and the downdip change to thin-bedded turbidites led van der Merwe et al. (2014) to interpret E2 as an intraslope lobe in the Geelbek area. The three divisions of E2 in Geelbek are interpreted here as lobe deposits that stack to form a lobe complex. In E2A, sandstones beds with bidirectional palaeocurrents and up-dip thinning are interpreted to indicate deflection of the flow column (Edwards et al., 1994). Soft-sediment deformation was triggered either through instability on the open erosional slope or through dewatering due to deposition of overlying strata. This range of features is consistent with a confined setting at the onset of the filling of slope accommodation. The amalgamated deposits of E2B are interpreted to be deposited in a scoured lobe-axis setting. The scour-fill interpretation is preferred to a channel-fill interpretation because no mudstone clast conglomerate facies is observed, the geometries of the structureless sandstone beds are tabular and can be walked out for ~1.5 km away, and the erosion surface shallows in the direction of main palaeocurrent direction. E2C is the most laterally extensive of the subunits. Lack of bidirectional palaeocurrent indicators and dominance of climbing-ripple laminated medium-bedded sandstones indicates a relatively unconfined phase of deposition. Overall, the depocentre of

518 successive E2 lobe deposits shifts slightly to the W (up slope; Fig. 9).
519 These findings conform to subsurface observations made in the Gulf
520 of Mexico indicating temporal evolution of the locus of
521 sedimentation (Prather et al., 2012b).

522

523

524 **6. Discussion**

525 **6.1 Mechanisms of slope accommodations**

526 Typically, submarine slope systems are dominated by sediment
527 bypass (e.g., Beaubouef et al., 1999; Gardner et al., 2003; Romans et
528 al., 2009; Hodgson et al., 2011). For lobate bodies to deposit on the
529 submarine slope low gradient areas of high accommodation must be
530 present. Here, the origin of this accommodation is discussed.

531 The formation of the intraslope lobe complexes of Unit D/E and
532 Subunit E1 in a similar location, albeit slightly offset, demonstrates
533 the presence of accommodation on Zoutkloof part of the
534 palaeoslope through multiple depositional sequences. In the
535 Zoutkloof area, there is no evidence of slide scars, syn-sedimentary
536 tectonic or diapiric deformation of the seabed, or underlying mass
537 transport complexes that could form an area of high
538 accommodation (Figueiredo et al., 2010). However, in the
539 underlying successions (Units A-D) the Zoutkloof area represents an
540 overall off-axis position with abundant silt-prone deposits (levees
541 and lobe fringes), and the main slope channel-levee systems to the

south (e.g., Grecula et al., 2003 a; Sixsmith et al., 2004; Figueiredo et al., 2010) feeding sand-prone basin-floor lobe complexes to the east and north east (Di Celma et al., 2011; van der Merwe et al., 2014). Therefore, slope accommodation at Zoutkloof is interpreted to be the result of differential compaction of the underlying fine grained stratigraphy relative to the more sand-rich underlying stratigraphy to the south (Figueiredo et al., 2010) and east (van der Merwe et al., 2014).

The geometries of architectural elements, palaeocurrent measurements, and facies distributions in Subunit E2 indicate a depositional setting that evolved from highly- to weakly-confined. E2A deposited on the partially healed accommodation (Fig. 10) and beds show evidence for flow deflection and reflection. E2B deposits show a slightly different main palaeocurrent direction and formed above an erosion surface that cuts into E2A and shallows downdip (Fig. 10). E2C shows onlap against the open slope when the accommodation was infilled (Fig. 10).

At the regional-scale, sedimentary features in the Geelbek area have been shown to form part of a step in a stepped slope profile with a ramp and sediment bypass ~ 2 km basinward of this area (van der Merwe et al., 2014). A large slide scar has been interpreted at the top of the underlying Unit D in this locality (Brunt et al., 2013b). In this study, an abrupt facies change from claystones with a clast-rich sandstone marker bed to a 30 m-thick asymmetric wedge of thin-bedded siltstone (Fig. 8) in strata underlying Subunit E2 has been

identified. This is interpreted to indicate the presence of a W-E oriented slide scar that formed near the step-to-ramp transition area prior to the initiation of Unit E, but was only partially healed, and could have modified and amplified the accommodation for the E2 intraslope lobe complex (Fig. 10).

6.2 Diagnostic criteria for intraslope lobe deposits

The identification of key characteristics of intraslope lobes compared to basin floor lobes can aid their identification in less well constrained subsurface and outcrop datasets (Fig. 11a). Geometries and architecture have been compared using published data from basin floor lobes in the Karoo Basin (Fan 3, Tanqua depocentre, Prélat et al., 2009; Unit A, Laingsburg depocentre, Prélat and Hodgson, 2013) with intraslope lobes of Units D/E and E (Table 1).

6.2.1 Dimensions

The lobe complexes are 6 to 10 km wide, 15 to 25 km long and 10 to 15 m thick. In volume, they are an order of magnitude smaller than dimensions of basin floor lobe complexes quoted in Prélat et al. (2010), which are 10 to 30 km wide and 30 to 100 m thick.

6.2.2 Lobe stacking patterns

Lobes stack to form lobe complexes (Deptuck et al., 2008; Prélat et al., 2009), and the patterns of stacking of lobes within such complexes provide an insight into the degree of confinement

590 (Deptuck et al., 2008; Straub et al., 2009). Generally, an
591 aggradational to slightly compensational style of stacking is
592 observed within intraslope lobes of the Fort Brown Formation (Fig.
593 11). This characteristic is also identified from subsurface studies of
594 recent deepwater systems (Ferry et al., 2005; Barton, 2012). In
595 contrast, basin floor lobes exhibit markedly compensational styles of
596 stacking, indicative of relatively unconfined settings (Prélat et al.,
597 2009; Straub et al., 2009; Groenenberg et al., 2010).

598 ***6.2.3 Sedimentary facies and features***

599 Intraslope lobe-axis deposits share similar facies associations with
600 basin floor lobes (e.g., Prélat et al., 2009). Off-axis deposits of
601 intraslope lobes are characterised by an abundance of medium
602 bedded ripple- and climbing ripple-laminated sandstones (Fig. 11).
603 Successions of climbing-wavy-climbing lamination or ripple-wavy-
604 ripple lamination are indicative of highly unsteady flows with high
605 rates of sediment fallout. Individual beds can preserve ripple forms
606 and climbing ripple-lamination that yield palaeoflow directions
607 oriented at a high angle or even opposite to each other (Fig. 11),
608 indicating deflection and reflection of the turbidity current during
609 sedimentation. Commonly, basin floor, lobe fringe deposits contain
610 numerous bipartite beds (Hodgson, 2009), and these are relatively
611 rare in intraslope lobe fringe deposits. Erosion surfaces mantled
612 with mudclasts are more common in intraslope lobe axis and lobe
613 off-axis deposits than in basin floor lobe systems because proximity
614 to channels and flow confinement leads to more entrainment of

615 fine-grained substrate. Basin floor lobes also display erosion
616 surfaces in the lobe axis, leading to amalgamation of thick-bedded
617 sandstones by removal of intervening thin beds (Stephen et al.,
618 2001; Prélat et al., 2009). However, erosion surfaces in basin floor
619 lobes are more subtle than in the intraslope lobes. In basin floor
620 lobe systems, facies transitions occur over several kilometres, both
621 frontally and laterally (e.g., Prélat et al., 2009; Groenenberg et al.,
622 2010), whereas in intraslope lobe systems, facies transitions occur
623 over shorter distances (typically over 10+ m), as observed in Unit E2
624 in the Geelbek area (Fig. 9).

625 ***6.2.4 Sand percentage***

626 Overall, intraslope lobe deposits are characterised by a higher
627 percentage of sandstone than basin floor lobe deposits because
628 sand becomes trapped preferentially in areas where available
629 accommodation is limited compared to flow depth (Brunt et al.,
630 2004). If the flow height is greater than the relief of the confinement
631 then the upper fine-grained part of the flow can be stripped, which
632 will increase the proportion of sand that is accumulated (Sinclair and
633 Tomasso, 2002; Prather et al., 2012b). Basin floor lobes of Unit A
634 have an average sandstone percentage of 60% , with >80% in lobe
635 axes and < 40% in distal lobe fringe settings (Prélat et al., 2009);
636 intraslope lobes of Unit D/E and E show an average of 75%
637 sandstone, with >90% in lobe axes and <50 % sandstone in lobe
638 fringes (Table 1, Fig. 11b).

639 ***6.2.5. Incision of intraslope lobes by channels***

Commonly, intraslope lobes are incised by channels (e.g., Adeogba et al., 2005). Incision of the E1 lobe complex by low-aspect-ratio channel systems of different ages, including E1-aged channels, indicates that when the accommodation had been filled, slope channel systems could develop in response to a lower base level. This indicates that slope accommodation in this area was transient. This is supported by the identification of thick basin floor lobe complexes of Unit E age farther into the basin by van der Merwe et al. (2014).

7. Conclusions

Three exhumed intraslope lobe complexes, constrained by stratigraphic and geographic position based on extensive and detailed correlation and mapping in the Laingsburg depocentre, Karoo Basin, were studied to establish their sedimentological and stratigraphic characteristics.

In the study area, intraslope lobe complexes are a 6 to 10 km wide and extend 15 to 25 km in down-dip directions; areal extent is controlled by the area over which slope accommodation was generated. The deposits are sandstone-rich and lack significant siltstone. Stacking patterns are aggradational to slightly compensational depending on the amount of confinement. The lobe axis is dominated by thick-bedded, amalgamated sandstones. The lobe off-axis mainly comprises medium-bedded climbing-ripple laminated sandstones. The lobe fringe is characterised by ripple- and climbing ripple-laminated sandstones that can show flow deflection

665 and reflection, and are interbedded with siltstones. Lateral and
666 vertical facies changes occur over tens of metres and demonstrate
667 highly variable, unsteady depositional flows that interacted with,
668 and were governed by, underlying sea-bed topography and
669 surrounding confinement. Two mechanisms are identified for the
670 development of accommodation on the Karoo slope: differential
671 compaction and scars formed by mass wasting processes. The
672 presence of intraslope lobe complexes supports regional
673 interpretations that the slope of the Laingsburg depocentre
674 developed a series of steps. These sub-seismic-scale observations
675 and interpretations provide possible analogues to sub-surface
676 examples identified on geophysical data for which information
677 relating to detailed internal sedimentary architecture is not
678 available.

679 The development of sedimentological and stratigraphic recognition
680 criteria for identification of intraslope lobes will permit improved
681 reconstruction of the stratigraphic evolution of continental margins.
682 However, the depositional architecture will vary across systems
683 depending on the mechanism responsible for slope accommodation,
684 the areal extent of the accommodation, and the ratio of flow size
685 and the degree of confinement.

686

687 **Acknowledgements**

The authors thank the local farmers of the Laingsburg region for permission to undertake field studies on their land. We thank Riccardo Teloni, Menno Hofstra, and Mariana Gomez O'Connell for field assistance. Christopher Stevenson is acknowledged for constructive discussion of the manuscript. The LOBE 2 project is funded by an industry consortium (Anadarko, BayernGas Norge, BG Group, BHPBilliton, BP, Chevron, DONG Energy, E.ON, Gaz de France-Suez, Maersk, Marathon, Shell, Statoil, Total, VNG Norge, and Woodside). Reviews by the Sedimentary Geology Editor-in-Chief Jasper Knight and the reviewers Fabiano Gamberi and Marzia Rovere have greatly improved the manuscript.

References

Adeogba, A.A., McHargue, T.R., Graham, S.A., 2005. Transient fan architecture and depositional controls from near-surface 3-D seismic data, Niger Delta continental slope. AAPG Bulletin 89, 627-643.

Allen, J.R.L., 1971. Instantaneous sediment deposition rates deduced from climbing-ripple cross-lamination. Journal of the Geological Society 127, 553-561.

Allen, J.R.L., 1982. Sedimentary Structures: Their Character and Physical Basis, Vols. 1, 2. Amsterdam, Elsevier, 593pp, 663pp.

Arnott, R.W.C., Hand, B.C., 1989. Bedforms, Primary Structures and Grain Fabric in the Presence of Suspended Sediment Rain. Journal of Sedimentary Petrology 59, 1062-1069.

712 Barton, M.D., 2012. Evolution of an Intra-Slope Apron, Offshore
713 Niger Delta Slope: Impact of Step Geometry on Apron Architecture.
714 In: Prather, B.E., Deptuck, M.E., Mohrig, D., van Hoorn, B., Wynn,
715 R.B. (Eds.), Application of the Principles of Seismic Geomorphology
716 to Continental -Slope and Base-of-Slope Systems: Case Studies from
717 Seafloor and Near-Seafloor Analogues. SEPM Special Publication 99,
718 pp. 181- 197.

719 Beaubouef, R.T., Rossen, C., Lovell, R.W.W., 2007. The Beacon
720 Channel: A newly Recognized Architectural Type in the Brushy
721 Canyon Formation, Texas, USA. In: Nielsen, T.H., Shew, R.D.,
722 Steffens, G.S., Studlick, J.R.J. (Eds.). Atlas of Deep-Water Outcrops.
723 AAPG Studies in Geology 56. AAPG and Shell Exploration &
724 Production, pp. 432-444.

725 Beaubouef, R.T., Rossen, C., Zelt, F.B., Sullivan, M.D., Mohrig, D.C.,
726 and Jennette, D.C. 1999, Deep-water sandstones, Brushy Canyon
727 Formation, West Texas. AAPG Continuing Education Course Notes,
728 40, 50pp.

729 Bernhardt, A., Jobe, Z.R., Grove, M., Lowe, D.R., 2012.
730 Palaeogeography and diachronous infill of an ancient deep-marine
731 foreland basin, Upper Cretaceous Cerro Toro Formation, Magallanes
732 Basin, Chile. Basin Research 24, 269-294.

733 Best, J., Bridge, J., 1992. The morphology and dynamics of low
734 amplitude bedwaves upon upper stage plane beds and the
735 preservation of planar laminae. Sedimentology 39, 737-752.

736 Booth, J.R., Dean, M.C., DuVernay, A.E., Styzen, M.J., 2003. Paleo-
737 bathymetric controls on the stratigraphic architecture and reservoir
738 development of confined fans in the Auger Basin: central Gulf of
739 Mexico slope. Marine and Petroleum Geology 20, 563-586.

740 Bouma, A.H., 1962. Sedimentology of some flysch deposits: a
741 graphic approach to facies interpretation. Elsevier, Amsterdam,
742 168pp.

743 Brunt, R.L., Hodgson, D.M., Flint, S.S., Pringle, J.K., Di Celma, C.,
744 Prélat, A., Grecula, M., 2013a. Confined to unconfined: Anatomy of a
745 base of slope succession, Karoo Basin, South Africa. Marine and
746 Petroleum Geology 41, 206-221.

747 Brunt, R.L., Di Celma, C.N., Hodgson, D.M., Flint, S.S., Kavanagh, J.P.,
748 van der Merwe, W.C., 2013b. Driving a channel through the levee
749 when the levee is high: An outcrop example of submarine down-dip
750 entrenchment. Marine and Petroleum Geology 41, 134-145.

751 Brunt, R.L., McCaffrey, W.D., Kneller, B.C., 2004. Experimental
752 Modeling of the Spatial Distribution of Grain Size Developed in a Fill-
753 and- Spill Mini-Basin Setting. Journal of Sedimentary Research 74,
754 438-446.

755 Burgreen, B., Graham, S., 2014. Evolution of a deep-water lobe
756 system in the Neogene trench-slope setting of the East Coast Basin,
757 New Zealand: lobe stratigraphy and architecture in a weakly
758 confined basin configuration. Marine and Petroleum Geology 54, 1-
759 22.

760 Catuneanu, O., Hancox, P.J., Rubidge, B.S., 1998. Reciprocal flexural
761 behaviour and contrasting stratigraphies: a new basin development
762 model for the Karoo retroarc foreland system, South Africa. Basin
763 Research 10, 417-439.

764 Deptuck, M.E., Piper, D.J.W., Savoye, B., Gervais, A., 2008.
765 Dimensions and architecture of late Pleistocene submarine lobes off
766 the northern margin of East Corsica. Sedimentology 55, 869-898.

767 Di Celma, C.N., Brunt, R.L., Hodgson, D.M., Flint, S.S., Kavanagh, J.P.,
768 2011. Spatial and Temporal Evolution of a Permian Submarine Slope
769 Channel-Levee System, Karoo Basin, South Africa. Journal of
770 Sedimentary Research 81, 579-599.

771 Edwards, D.A., Leeder, M.R., Best, J.L., Pantin, H.M., 1994. On
772 experimental reflected density currents and the interpretation of
773 certain turbidites. Sedimentology 41, 437- 461.

774 Eschard, R., Albouy, E., Gaumet, F., Ayub, A., 2004. Comparing the
775 depositional architecture of basin floor fans and slope fans in the
776 Pab Sandstone, Maastrichtian, Pakistan. In: Lomas, S.A. (Ed.),
777 Confined Turbidite Systems. Geological Society of London, Special
778 Publications 222, pp. 159-185.

779 Etienne, S., Mulder, T., Bez, M., Desaubliaux, G., Kwasniewski, A.,
780 Parize, O., Dujoncquoy, E., Salles, T., 2012. Multiple scale
781 characterization of sand-rich distal lobe deposit variability: Examples
782 from the Annot Sandstones Formation, Eocene–Oligocene, SE
783 France. Sedimentary Geology 273-274, 1-18.

784 Ferry, J.N., Mulder, T., Parize, O., Raillard, S., 2005. Concept of
785 equilibrium profile in deep-water turbidite system: effects of local
786 physiographic changes on the nature of sedimentary process and
787 the geometries of deposits. In: Hodgson, D.M., Flint, S.S. (Eds.),
788 Submarine Slope Systems: Processes and Products, Geological
789 Society of London, Special Publications 244, pp. 181-193.

790 Fiduk, J.C., Weimer, P., Trudgill, B.D., Rowan, M.G., Gale, P.E., Phair,
791 R.L., Korn, B.E., Roberts, G.R., Gafford, W.T., Lowe, R.S., 1999. The
792 Perdido fold belt, northwestern deep Gulf of Mexico, part 2: seismic
793 stratigraphy and petroleum systems. AAPG Bulletin 83, 578-612.

794 Figueiredo, J.J.P., Hodgson, D.M., Flint, S.S., Kavanagh, J.P., 2010.
795 Depositional Environments and Sequence Stratigraphy of an
796 Exhumed Permian Mudstone-Dominated Submarine Slope
797 Succession, Karoo Basin, South Africa. Journal of Sedimentary
798 Research 80, 97-118.

799 Figueiredo, J.J.P., Hodgson, D.M., Flint, S.S., Kavanagh, J.P., 2013.
800 Architecture of a channel complex formed and filled during long-
801 term degradation and entrenchment on the upper submarine slope,
802 Unit F, Fort Brown Fm., SW Karoo Basin, South Africa. Marine and
803 Petroleum Geology 41, 104-116.

804 Flint, S.S., Hodgson, D.M., Sprague, A.R., Brunt, R.L., van der Merwe,
805 W.C., Figueiredo, J., Prélat, A., Box, D., Di Celma, C., Kavanagh, J.P.,
806 2011. Depositional architecture and sequence stratigraphy of the

807 Karoo basin floor to shelf edge succession, Laingsburg depocentre,
808 South Africa. Marine and Petroleum Geology 28, 658-674.

809 Gamberi, F., Rovere, M., 2011. Architecture of a modern transient
810 slope fan (Villafranca fan, Gioia basin–Southeastern Tyrrhenian Sea).
811 Sedimentary Geology 236, 211-225.

812 Gamberi, F., Rovere, M., Marani, M., 2011. Mass-transport complex
813 evolution in a tectonically active margin (Gioia Basin, Southeastern
814 Tyrrhenian Sea). Marine Geology 279, 98-110.

815 Gardner, M.H., Borer, J.A., Melick, J.J., Mavilla, N., Dechesne, M.,
816 and Wagerle, R.N. 2003, Stratigraphic process-response model for
817 submarine channels and related features from studies of Permian
818 Brushy Canyon outcrops, West Texas. Marine and Petroleum
819 Geology, 20, 757-787.

820 Grecula, M., Flint, S.S., Wickens, H.D.V., Johnson, S.D., 2003a.
821 Upward-thickening patterns and lateral continuity of Permian sand-
822 rich turbidite channel fills, Laingsburg Karoo, South Africa.
823 Sedimentology 50, 831-853.

824 Grecula, M., Flint, S., Potts, G., Wickens, D., Johnson, S., 2003b.
825 Partial Ponding of Turbidite Systems in a Basin with Subtle Growth-
826 Fault Topography: Laingsburg-Karoo, South Africa. Journal of
827 Sedimentary Research 73, 603-620.

828 Groenenberg, R.M., Hodgson, D.M., Prélat, A., Luthi, S.M., Flint, S.S.,
829 2010. Flow-Deposit Interaction in Submarine Lobes: Insights from

830 Outcrop Observations and Realizations of a Process-Based
831 Numerical Model. Journal of Sedimentary Research 80, 252-267.

832 Grundvåg, S.A., Johannessen, E.P., Helland-Hansen, W., Plink-
833 Björklund, P., 2014. Depositional architecture and evolution of
834 progradationally stacked lobe complexes in the Eocene Central Basin
835 of Spitsbergen. Sedimentology 61, 535-569.

836 Hartog Jager, D.D., Giles, M.R., Griffiths, G.R., 1993. Evolution of
837 Paleogene submarine fans of the North Sea in space and time. In:
838 Parker, J.R. (Ed.), Petroleum Geology of Northwest Europe:
839 Proceedings of the 4th Conference, Geological Society of London,
840 London, pp. 59-71.

841 Haughton, P., Davis, C., McCaffrey, W., Barker, S., 2009. Hybrid
842 sediment gravity flow deposits – Classification, origin and
843 significance. Marine and Petroleum Geology 26, 1900-1918.

844 Hodgson, D.M., 2009. Distribution and origin of hybrid beds in sand-
845 rich submarine fans of the Tanqua depocentre, Karoo Basin, South
846 Africa. Marine and Petroleum Geology 26, 1940-1956.

847 Hodgson, D.M., Di Celma, C.N., Brunt, R.L., Flint, S.S., 2011.
848 Submarine slope degradation and aggradation and the stratigraphic
849 evolution of channel-levee systems. Journal of the Geological
850 Society 168, 625-628.

851 Harms, J.C., 1974. Brushy Canyon Formation, Texas: A Deep-Water
852 Density Current Deposit. Bulletin of the Geological Society of
853 America 85, 1763-1784.

854 Ito, M., 2008. Downfan Transformation from Turbidity Currents to
855 Debris Flows at a Channel-to-Lobe Transitional Zone: The Lower
856 Pleistocene Otadai Formation, Boso Peninsula, Japan. Journal of
857 Sedimentary Research 78, 668-682.

858 Jobe, Z.R., Lowe, D.R., Morris, W.R., 2012. Climbing-ripple
859 successions in turbidite systems: depositional environments,
860 sedimentation rates and accumulation times. Sedimentology 59,
861 867-898.

862 Kane, I.A., Hodgson, D.M., 2011. Sedimentological criteria to
863 differentiate submarine channel levee subenvironments: Exhumed
864 examples from Rosario Fm. (Upper Cretaceous) Baja California,
865 Mexico, and Fort Brown Fm. (Permian), Karoo Basin, S. Africa.
866 Marine and Petroleum Geology 28, 807-823.
867

868 Kilhams, B., Hartley, A., Huuse, M., Davis, C., 2012. Characterizing
869 the Paleocene turbidites of the North Sea: the Mey Sandstone
870 Member, Lista Formation, UK Central Graben. Petroleum
871 Geoscience 18, 337-354.

872 Kneller, B.C., Branney, M.J., 1995. Sustained high-density turbidity
873 currents and the deposition of thick massive sands. Sedimentology
874 42, 607-616.

875 Komar, P.D., 1971. Hydraulic Jumps in Turbidity Currents. AAPG
876 Bulletin 82, 1477-1487.

877 Leclair, S.F., Arnott, R.W.C., 2005. Parallel Lamination Formed by
878 High-Density Turbidity Currents. Journal of Sedimentary Research
879 75, 1-5.

880 Li, L., Wang, Y., Xu, Q., Zhao, J., Li, D., 2012. Seismic geomorphology
881 and main controls of deep-water gravity flow sedimentary process
882 on the slope of the northern South China Sea. Science China Earth
883 Sciences 55, 747-757.

884 Li, L., Wang, Y. M., Zhang, L. M., Huang, Z. C., 2010. Confined gravity
885 flow sedimentary process and its impact on the lower continental
886 slope, Niger Delta. Science China Earth Sciences 53, 1169-1175.

887 Marchès, E., Mulder, T., Gonthier, E., Cremer, M., Hanquiez, V.,
888 Garlan, T., Lecroat, P., 2010. Perched lobe formation in the Gulf of
889 Cadiz: Interactions between gravity processes and contour currents
890 (Algarve Margin, Southern Portugal). Sedimentary Geology 229, 81-
891 94.

892 McCaffrey, W.D., Kneller, B.C., 2001. Process controls on the
893 development of stratigraphic trap potential on the margins of
894 confined turbidite systems and aids to reservoir evaluation. AAPG
895 Bulletin 85, 971-988.

896 McKay, M.P., Weislogel, A.L., Fildani, A., Brunt, R.L., Hodgson, D.M.,
897 Flint, S.S., 2015. U-PB zircon tuff geochronology from the Karoo
898 Basin, South Africa: implications of zircon recycling on stratigraphic
899 age controls. International Geology Review 57, 393-410.

900 Morris, E.A., Hodgson, D.M., Flint, S.S., Brunt, R.L., Butterworth, P.L.,
901 Verhaeghe, J., 2014a. Sedimentology, Stratigraphic Architecture and
902 Depositional Context of Submarine Frontal Lobe Complexes. Journal
903 of Sedimentary Research 84, 763-780.

904 Morris, E.A., Hodgson, D.M., Brunt, R.L., Flint, S.S. 2014b. Origin,
905 evolution and anatomy of silt-prone submarine external levées.
906 Sedimentology 61, 1734-1763.

907 Mulder, T., Alexander, J., 2001. Abrupt change in slope causes
908 variation in the deposit thickness of concentrated particle-driven
909 density currents. Marine Geology 175, 221-235.

910 Mutti, E., 1992. Turbidite Sandstones. Agip -Instituto di Geologia,
911 Università di Parma, Italy, 275pp.

912 Oluboyo, A.P., Gawthorpe, R.L., Bakke, K., Hadler-Jacobson, F., 2014.
913 Salt tectonic controls on deep-water turbidite depositional systems:
914 Miocene, southwestern Lower Congo Basin, offshore Angola. Basin
915 Research 26, 597-620.

916 Pirmez, C., Prather, B.E., Mallarino, G., O'Hayer, W.W., Droxler,
917 A.W., Winker, C.D., 2012. Chronostratigraphy of the Brazos-Trinity
918 Depositional System, Western Gulf of Mexico: Implications for
919 Deepwater Depositional Models. In: Prather, B.E., Deptuck, M.E.,
920 Mohrig, D., van Hoorn, B., Wynn, R.B. (Eds.), Application of the
921 Principles of Seismic Geomorphology to Continental -Slope and
922 Base-of-Slope Systems: Case Studies from Seafloor and Near-
923 Seafloor Analogues. SEPM Special Publication 99, pp. 112-143.

924 Plink-Björklund, P., Steel, R., 2002. Sea-level fall below the shelf
925 edge, without basin-floor fans. Geology 30, 115-118.

926 Prather, B.E., Booth, J.R., Steffens, G.S., Craig, P.A., 1998.
927 Classification, Lithologic Calibration, and Stratigraphic Succession of
928 Seismic Facies of Intraslope Basins, Deep-Water Gulf of Mexico.
929 AAPG Bulletin 82, 701-728.

930 Prather, B.E., Pirmez, C., Sylvester, Z., Prather, D.S., 2012a.
931 Stratigraphic Response to Evolving Geomorphology in a Submarine
932 Apron Perched on the Upper Niger Delta Slope. In: Prather, B.E.,
933 Deptuck, M.E., Mohrig, D., van Hoorn, B., Wynn, R.B. (Eds.),
934 Application of the Principles of Seismic Geomorphology to
935 Continental -Slope and Base-of-Slope Systems: Case Studies from
936 Seafloor and Near-Seafloor Analogues. SEPM Special Publication 99,
937 pp. 145-161.

938 Prather, B.E., Pirmez, C., Winker, C.D. 2012b. Stratigraphy of Linked
939 Intraslope Basins: Brazos-Trinity System Western Gulf of Mexico. In:
940 Prather, B.E., Deptuck, M.E., Mohrig, D., van Hoorn, B., Wynn, R.B.
941 (Eds.), Application of the Principles of Seismic Geomorphology to
942 Continental -Slope and Base-of-Slope Systems: Case Studies from
943 Seafloor and Near-Seafloor Analogues. SEPM Special Publication 99,
944 pp. 83- 109.

945 Prélat, A., Hodgson, D.M., 2013. The full range of turbidite bed
946 thickness patterns in submarine lobes: controls and implications.
947 Journal of Geological Society of London 170, 1-6.

948 Prélat, A., Hodgson, D.M., Flint, S.S., 2009. Evolution, architecture
949 and hierarchy of distributary deep-water deposits: a high-resolution
950 outcrop investigation from the Permian Karoo Basin, South Africa.
951 Sedimentology 56, 2132-2154.

952 Prélat, A., Covault, J.A., Hodgson, D.M., Fildani, A., Flint, S.S. 2010.
953 Intrinsic controls on the range of volumes, morphologies, and
954 dimensions of submarine lobes. Sedimentary Geology 232, 66-76.

955 Pyles, D.R., 2008. Multiscale stratigraphic analysis of a structurally
956 confined submarine fan: Carboniferous Ross Sandstone, Ireland.
957 AAPG Bulletin 92, 557-587.

958 Pyles, D.R., Jennette, D.C., 2009. Geometry and architectural
959 associations of co-genetic debrite–turbidite beds in basin-margin
960 strata, Carboniferous Ross Sandstone (Ireland): Applications to
961 reservoirs located on the margins of structurally confined submarine
962 fans. Marine and Petroleum Geology 26, 1974-1996.

963 Pysklywec, R.N., Mitrovica, J.X., 1999. The Role of Subduction-
964 Induced Subsidence in the Evolution of the Karoo Basin. The Journal
965 of Geology 107, 155-164.

966 Romans, B.W., Hubbard, S.M., and Graham, S.A. 2009, Stratigraphic
967 evolution of an outcropping continental slope system, Tres Pasos
968 Formation at Cerro Divisadero, Chile. Sedimentology 56, 737-764.

969 Sinclair, H.D., Tomasso, M., 2002. Depositional Evolution of Confined
970 Turbidite Basins. Journal of Sedimentary Research 72, 451-456.

971 Sixsmith, P.J., 2000. Stratigraphic development of a Permian
972 turbidite system on a deforming basin floor: Laingsburg Formation,
973 Karoo basin, South Africa. Ph.D. thesis, University of Liverpool,
974 Liverpool.

975 Sixsmith, P.J., Flint, S.S., Wickens, H.D., Johnson, S.D., 2004.
976 Anatomy and Stratigraphic Development of a Basin Floor Turbidite
977 System in the Laingsburg Formation, Main Karoo Basin, South Africa.
978 Journal of Sedimentary Research 74, 239-254.

979 Southard, J.B., 1991. Experimental determination of bed-Form
980 stability. Annual Review of Earth and Planetary Science 19, 423-55.

981 Stephen, K.D., Clark, J.D., Gardiner, A.R., 2001. Outcrop-based
982 stochastic modelling of turbidite amalgamation and its effects on
983 hydrocarbon recovery. Petroleum Geoscience 7, 163-172.

984 Stow, D.A.V., Piper, D.J.W., 1984. Deep-water fine-grained
985 sediments: facies models. In: Stow, D.A.V., Piper, D.J.W. (Eds.), Fine-
986 grained Sediments: Deep-water Processes and Facies. Geological
987 Societyof London, Special Publication 15, pp. 611-646.

988 Straub, K.M., Paola, C., Mohrig, D., Wolinsky, M.A., George, T., 2009.
989 Compensational Stacking of Channelized Sedimentary Deposits.
990 Journal of Sedimentary Research 79, 673-688.

991 Talling, P.J., Masson, D.G., Sumner, E.J., Malgesini, G., 2012.
992 Subaqueous sediment density flows: Depositional processes and
993 deposit types. Sedimentology 59, 1937-2003.

994 Tankard, A., Welsink, H., Aukes, P., Newton, R., Stettler, E., 2009.
995 Tectonic evolution of the Cape and Karoo basins of South Africa.
996 Marine and Petroleum Geology 26, 1379-1412.

997 van der Merwe, W.C., Hodgson, D.M., Brunt, R.L., Flint, S.S., 2014.
998 Depositional architecture of sand-attached and sand-detached
999 channel-lobe transition zones on an exhumed stepped slope
1000 mapped over a 2500 km^2 area. Geosphere 10, 1076-1093.

1001 Visser, J.N.J., 1997. Deglaciation sequences in the Permo-
1002 Carboniferous Karoo and Kalahari basins of the southern Africa: a
1003 toll in the analysis of cyclic glaciomarine basin fills. Sedimentology
1004 44, 507-521.

1005 Visser, J.N.J., Prackelt, H.E., 1996. Subduction, mega-shear systems
1006 and Late Palaeozoic basin development in the African segment of
1007 Gondwana. Geologische Rundschau 85, 632-646.

1008

1009 **Figure Captions**

1010 Table 1. Comparison chart of the main sedimentological and
1011 stratigraphic characteristics of intraslope lobes and basin-floor
1012 lobes.

1013 Fig. 1. Principal features of a stepped deep-water system. Two
1014 mechanisms to generate accommodation on the slope are shown:
1015 generation of a slope step due to tectonic faulting and above a scar
1016 of a mass transport complex (MTC).

Fig. 2. (A) The Laingsburg depocentre is located inboard of the Cape Fold Belt. Black square indicates the area of study. Satellite images taken from Google Earth. (B) Location of detailed study areas: Roggekraal and Zoutkloof in the North, Geelbek in the South. White squares indicate the zoom-in areas in (D) and (E). Shading corresponds to colours of boxes in C. (C) Schematic stratigraphic log sections of the Fort Brown Fm., Laingsburg Fm. and Waterford Fm. (Flint et al., 2011). Units D/E and E are highlighted by the black square. (D) Detailed view of the Zoutkloof and E) Geelbek study areas. White lines indicate outcrop exposure, black dots indicate positions of logged sections, and black boxed areas of detailed correlation panels (Figure 7).

Fig. 3. Representative photographs of sedimentary facies observed in the Zoutkloof area. (A) Thick-bedded amalgamated sandstones of the lobe axis (FA 1). Geologist for scale (1.6 m). (B) Climbing ripple-laminated, medium bedded, fine-grained sandstones, with some stoss-side preservation, in lobe off-axis (FA 2). Camera lens cover for scale. (C) Heterolithic packages of thin-bedded sandstones and siltstones in the lobe fringe (FA 3). Logging pole (0.5 m) with 10 cm gradations as scale. (D) Hybrid bed (FA 4). Camera lens cover as scale. (E) Siltstone package with intercalated sandstones (FA 5). Logging pole (2 m) with 10 cm gradations as scale. (F) Silty claystones (FA 6). Geologist for scale (1.6 m).

Fig. 4. Representative photographs and correlation panel of the intraslope lobe complexes of Unit D/E and E1 in the Zoutkloof area

and correlation panel for the Roggekraal N area. (A) Coarsening- and thickening-upward at the base of the intraslope lobe deposits in Unit D/E. Logging pole with 10 cm gradations as scale. (B) Roggekraal N correlation panel showing siltstone intervals that separate individual lobes in Subunit E1 and the two lobes of Unit D/E. Dashed red line represents erosion surface (C) Tabular geometries of Unit D/E and Subunit E1 in the Zoutkloof N area. The sand-prone units are separated by a ~11 m thick mudstone. (D) E1 channels cut down through E1 lobes and into the underlying claystone (Zoutkloof N).

Fig. 5. Correlation panels for Unit D/E and Subunit E1 in the Zoutkloof area. Overall axis of the lobe complexes of Unit D/E and Subunit E1 is located in the Roggekraal and Zoutkloof N areas. Towards the north and south lateral facies transitions can be observed and correspond to lobe off-axis and lobe fringe deposits. Note incision of Subunit E1 by younger channel-fills.

Fig. 6. Simplified palaeogeographic reconstruction of (1) Unit D/E and (2) overlying Subunit E1 in the Zoutkloof area. Flows show evidence for deflection and reflection.

Fig. 7. Representative photographs of the intraslope complex in the Geelbek area. (A) Bed showing climbing-ripple lamination with opposing flow direction patterns. Camera lens cover as scale. (B) Deformed mudstone interlayer with flames. Camera lens cover as scale. (C) E2B overlies E2A outside of the basal scour surface. Camera lens cover as scale. (D) E2B and E2C are separated by a thin

(0.1 to 0.2 m thick; indicated by orange overlay) siltstone interval. Geologist (1.6 m) as scale.

Fig. 8. Correlation of subunit E2 in the Geelbek area. Panel is hung from hemipelagic claystone between E2 and E3. Black boxes (A-D) indicate areas shown in detail in Figure 9. Note siltstone wedge within the mudstone interval which is interpreted to partially fill a slide scar.

Fig. 9. Details of the Geelbek correlation panel. (A) Detailed correlation panel of E2A. (B) Injected mudstone below E2A with geologist as scale. (C) Detailed correlation panel of the E2C onlap zone. ‘a’ marks amalgamation surfaces, ‘E’ erosion surfaces. (D) Example graphic log through high-amalgamation zone of E2B overlain by well bedded, structured sandstone beds of E2C.

Fig. 10. Simplified palaeogeographic reconstruction of subunit E2 in the Geelbek area. (1) slide removeshemipelagic claystone and marker bed 3 (MB3). Surface is steep in the west and shallows to the east. (2) thin-bedded siltstone beds partially infill scar, which is also draped by hemipelagic mudstone. (3) deposition of confined sediments of E2A. (4) E2B locally scours into E2A. (5) onlap of E2C deposits to the west. Slope feeder channels are not exposed in the field and therefore not displayed.

Fig. 11. (A) Block diagram showing the key recognition criteria of intraslope lobes. Aggradational to slightly compensational stacking patterns; onlap combined with injection onto mud-prone slope;

highly amalgamated zones in the lobe complex axis; subtle confinement leads to fringes that show aggradational stacking; high degree of confinement leads to preservation of beds with evidence of flow deflection, erosional based beds and abrupt facies changes; climbing-ripple lamination is the dominant facies of the lobe-off axis; incision by low-aspect-ratio channels that originate in the same unit as the intraslope lobes; more lobe deposits can be found down-dip on the basin-floor or on steps basinward on the slope. (B) Simplified logs of typical thicknesses and stacking patterns from lobe axis to lobe fringe (downdip and laterally) in intraslope lobes that are observed over a few kilometres. Note position of the schematic logs from fringe (1) to axis (4) in (A).

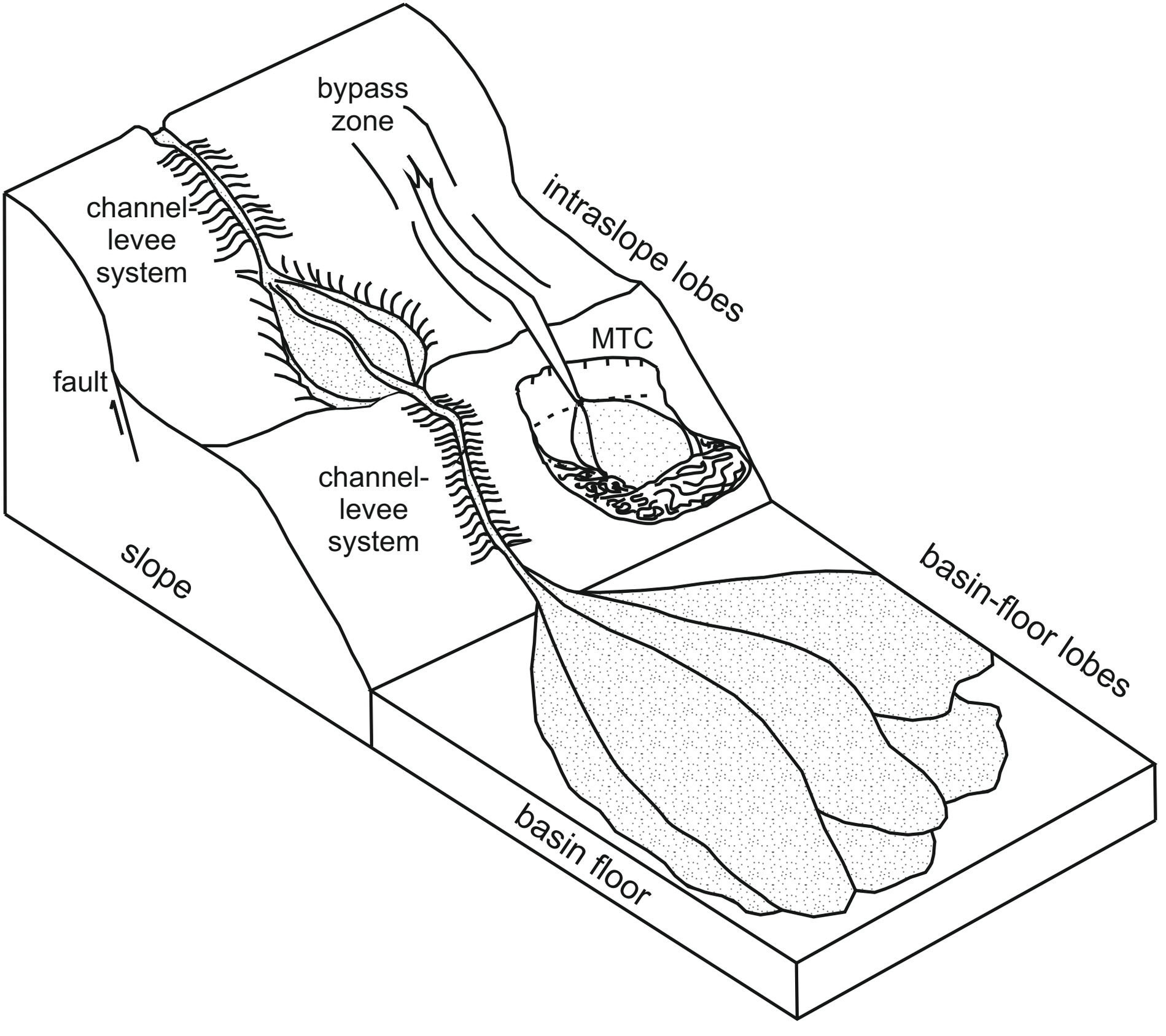
bypass
zone
channel-
levee
system
intraslope lobes
MTC
fault
channel-
levee
system
slope
basin-floor lobes
basin floor

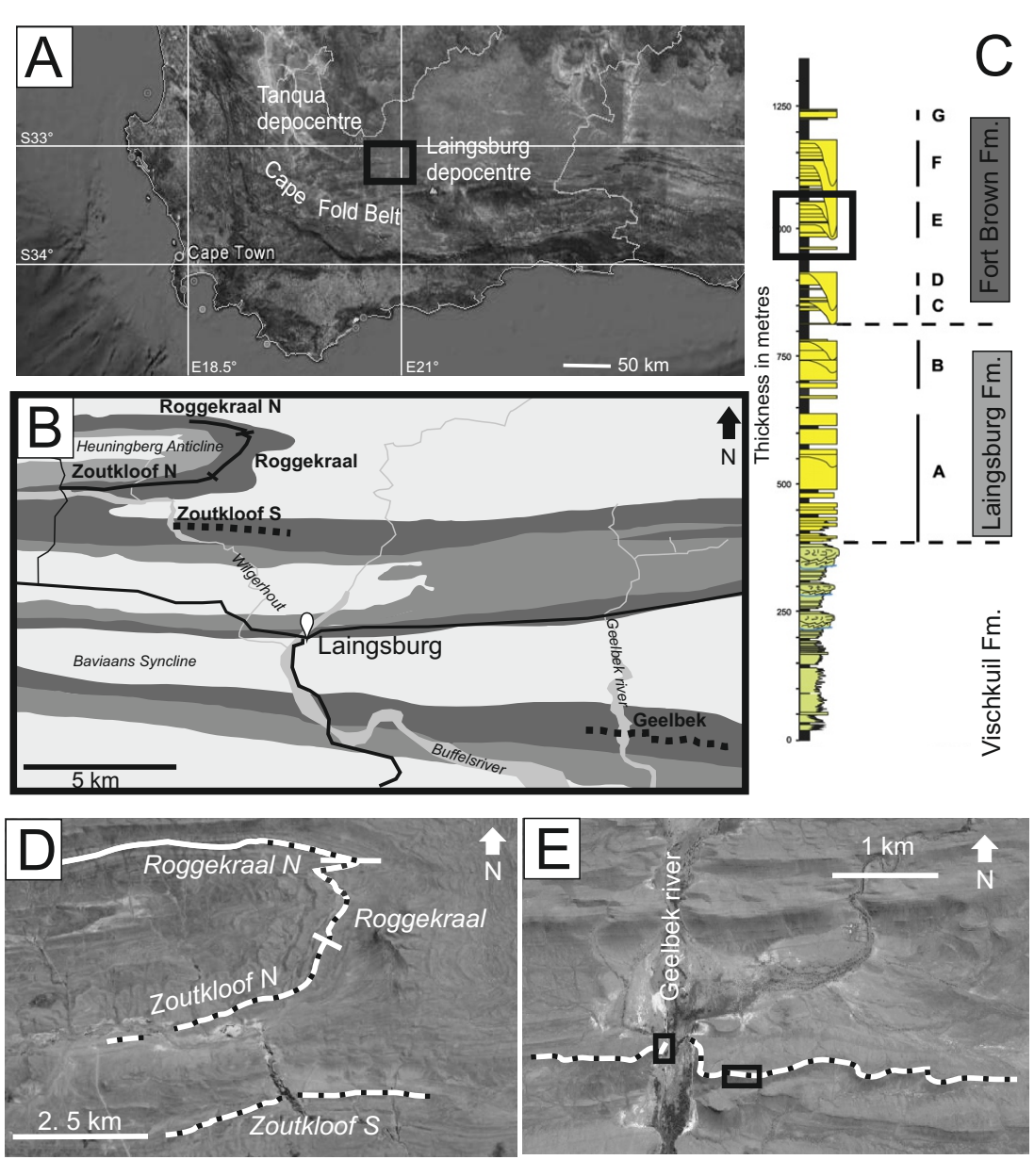
A
Tanqua
depocentre
Laingsburg
depocentre
Cape Fold Belt
S33°
S34°
Cape Town
E18.5°
E21°
50 km
B
Roggekraal N
Heuningberg Anticline
Roggekraal
Zoutkloof N
Zoutkloof S
Wilgerhout
Laingsburg
Baviaans Syncline
Geelbek river
Geelbek
Buffelsriver
5 km
N
C
Thickness in metres
1250
1000
750
500
250
0
G
F
E
D
C
B
A
Fort Brown Fm.
Laingsburg Fm.
Vischkuil Fm.
D
Roggekraal N
Roggekraal
Zoutkloof N
2. 5 km
Zoutkloof S
N
E
Geelbek river
1 km
N

FA1: thick-bedded sandstones
FA2: medium-bedded structured sandstones
FA3: heterolithic package
FA5:thin-bedded siltstones
FA6:hemipelagic claystones

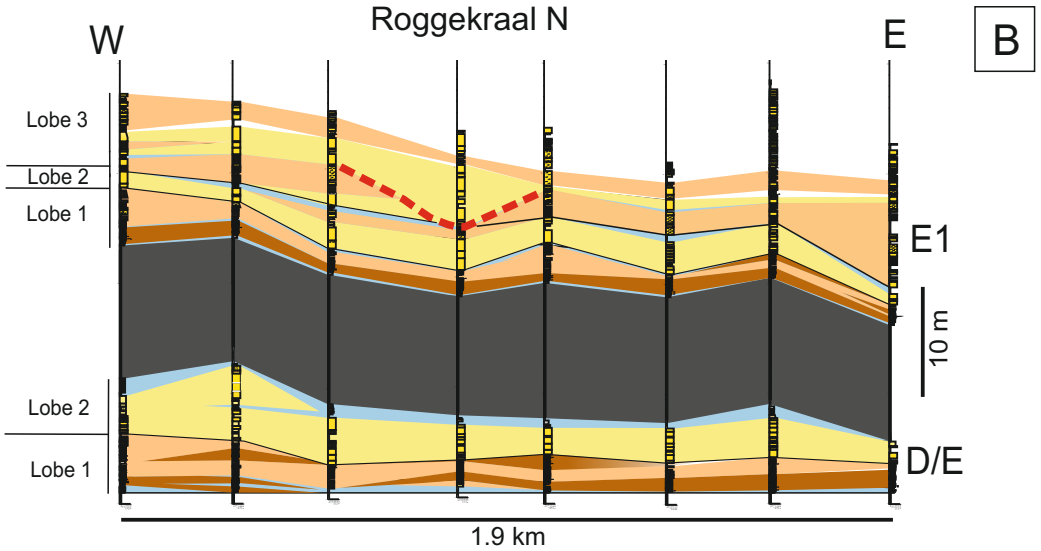

350 m

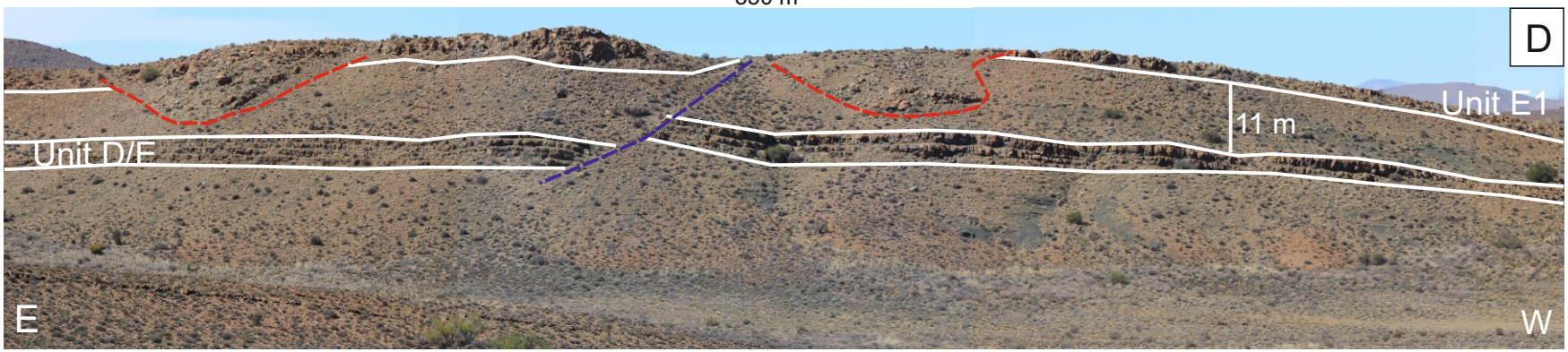

650 m

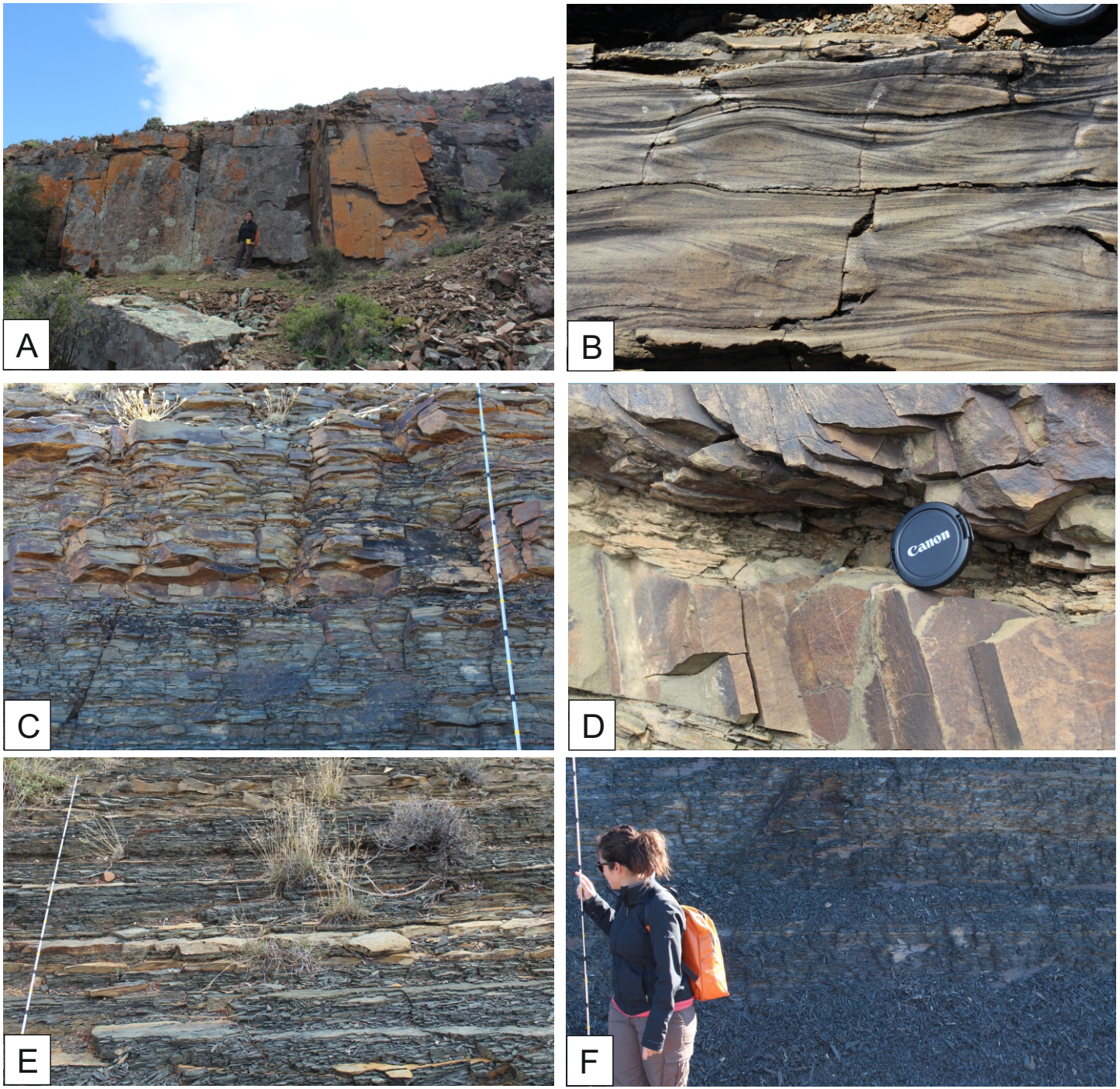
A
B
C
D
Canon
E
F

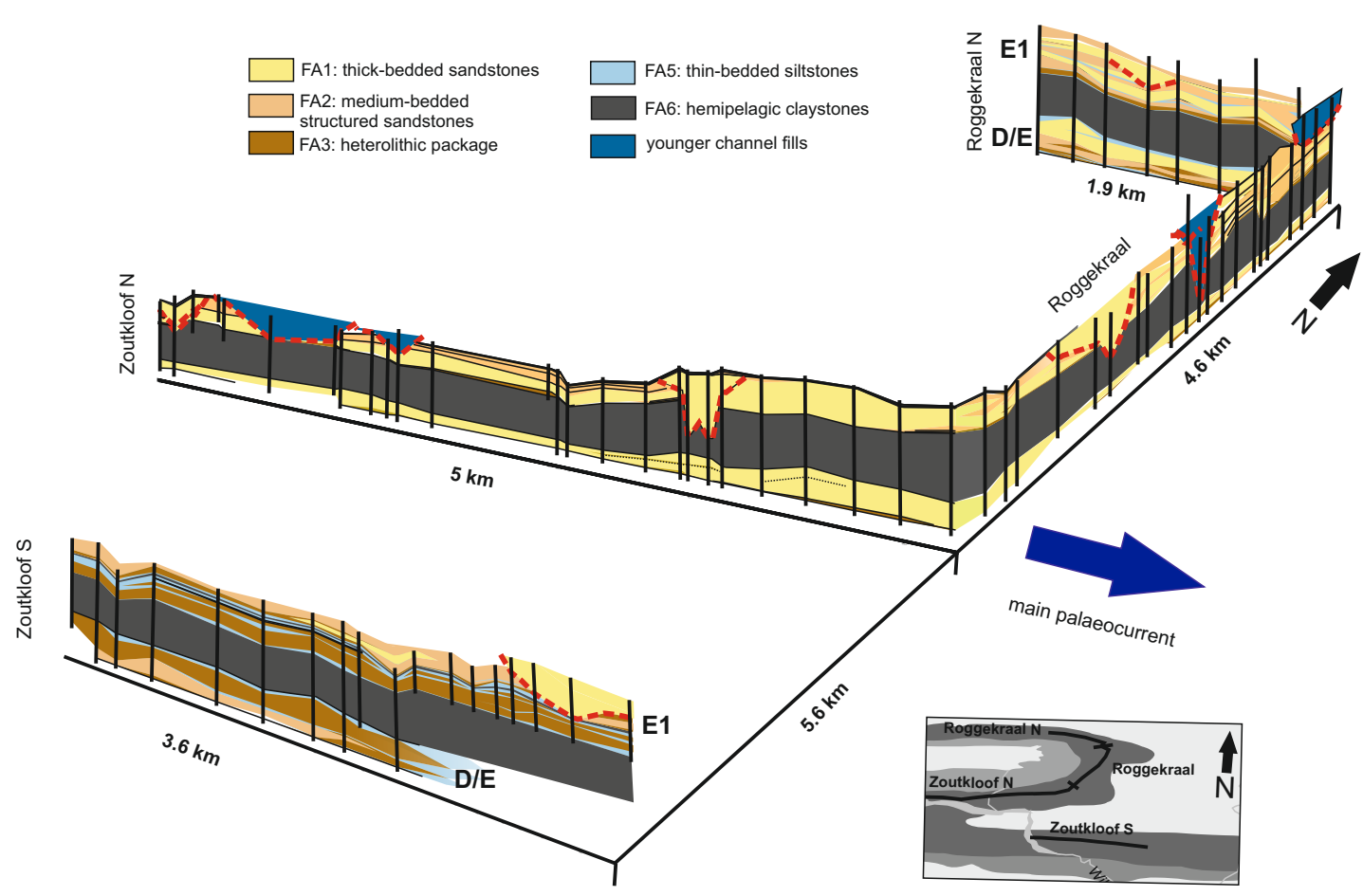
FA1: thick-bedded sandstones
FA2: medium-bedded structured sandstones
FA3: heterolithic package
FA5: thin-bedded siltstones
FA6: hemipelagic claystones
younger channel fills
Roggekraal N
E1
D/E
1.9 km
Zoutkloof N
Roggekraal
5 km
4.6 km
N
Zoutkloof S
3.6 km
E1
D/E
5.6 km
main palaeocurrent
Roggekraal N
Roggekraal
Zoutkloof N
Zoutkloof S
N

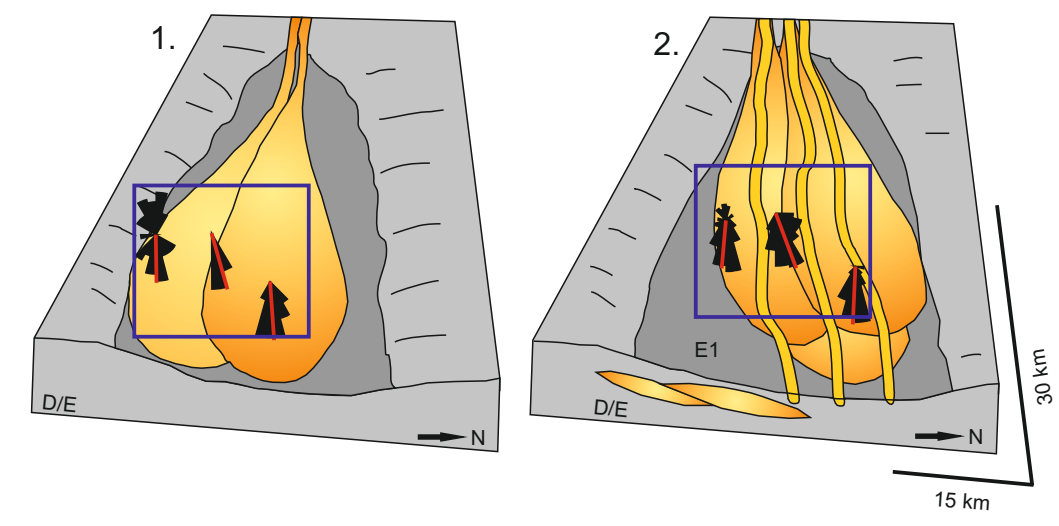
1.
D/E
N
2.
E1
D/E
N
30 km
15 km
hemipelagic background sedimentation
lobe deposits
channel fills
palaeocurrent measurements
study area

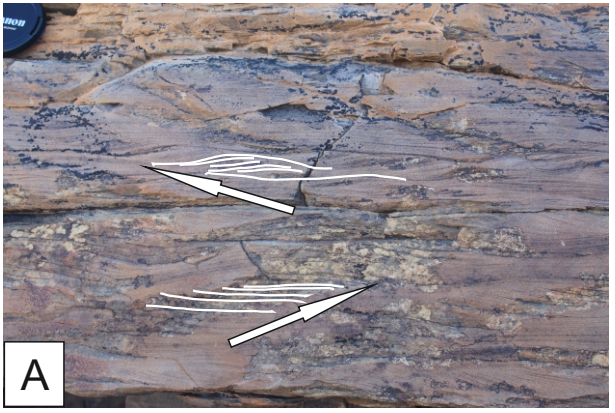
A


B


E2B
E2A
C


E2C
E2B
D

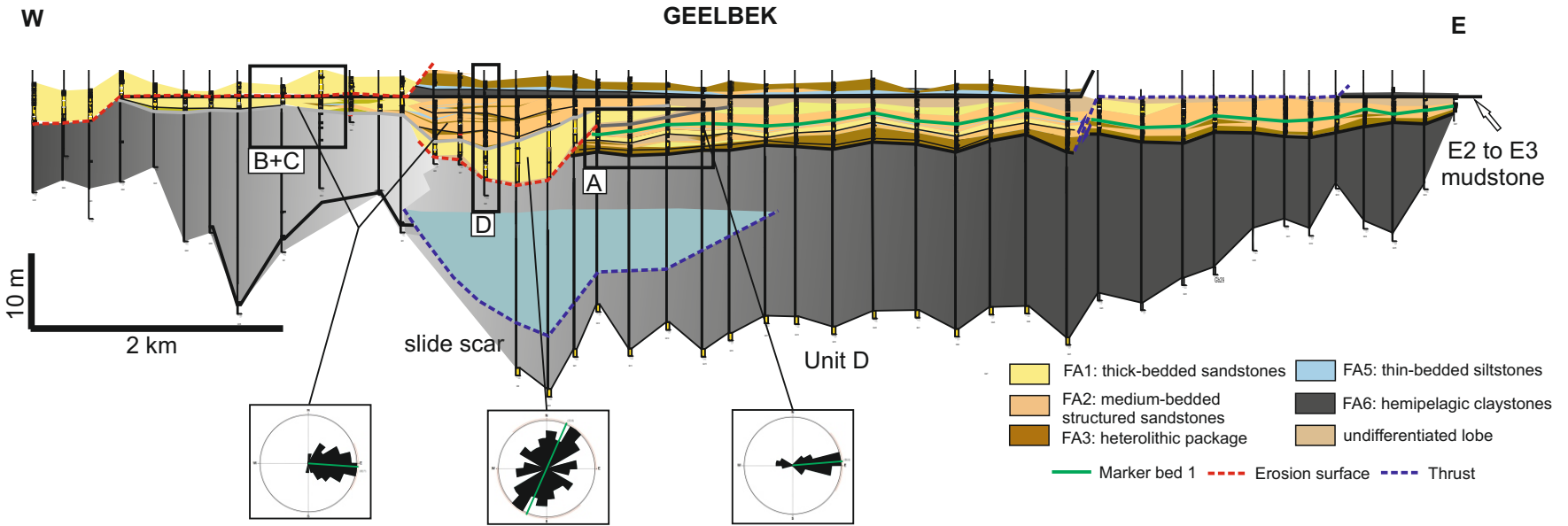
W
GEELBEK
E
B+C
A
D
E2 to E3
mudstone
10 m
2 km
slide scar
Unit D
FA1: thick-bedded sandstones
FA2: medium-bedded
structured sandstones
FA3: heterolithic package
FA5: thin-bedded siltstones
FA6: hemipelagic claystones
undifferentiated lobe
Marker bed 1
Erosion surface
Thrust

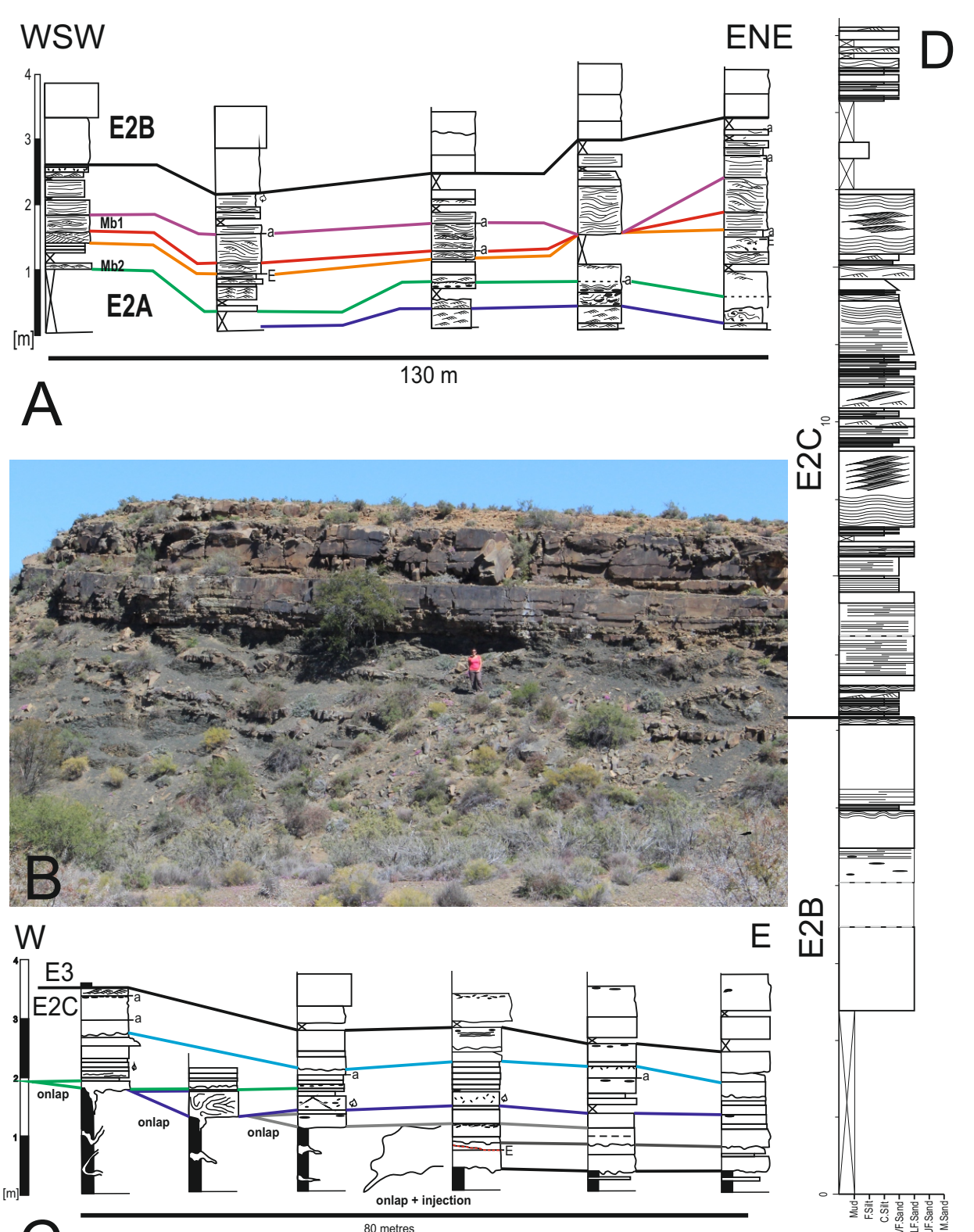
WSW
ENE
E2B
Mb1
Mb2
E2A
[m]
130 m
A
B
W
E
E3
E2C
onlap
onlap
onlap
onlap + injection
80 metres
C
D
E2C
E2B
Mud
F.Silt
C.Silt
VF.Sand
LF.Sand
UF.Sand
M.Sand

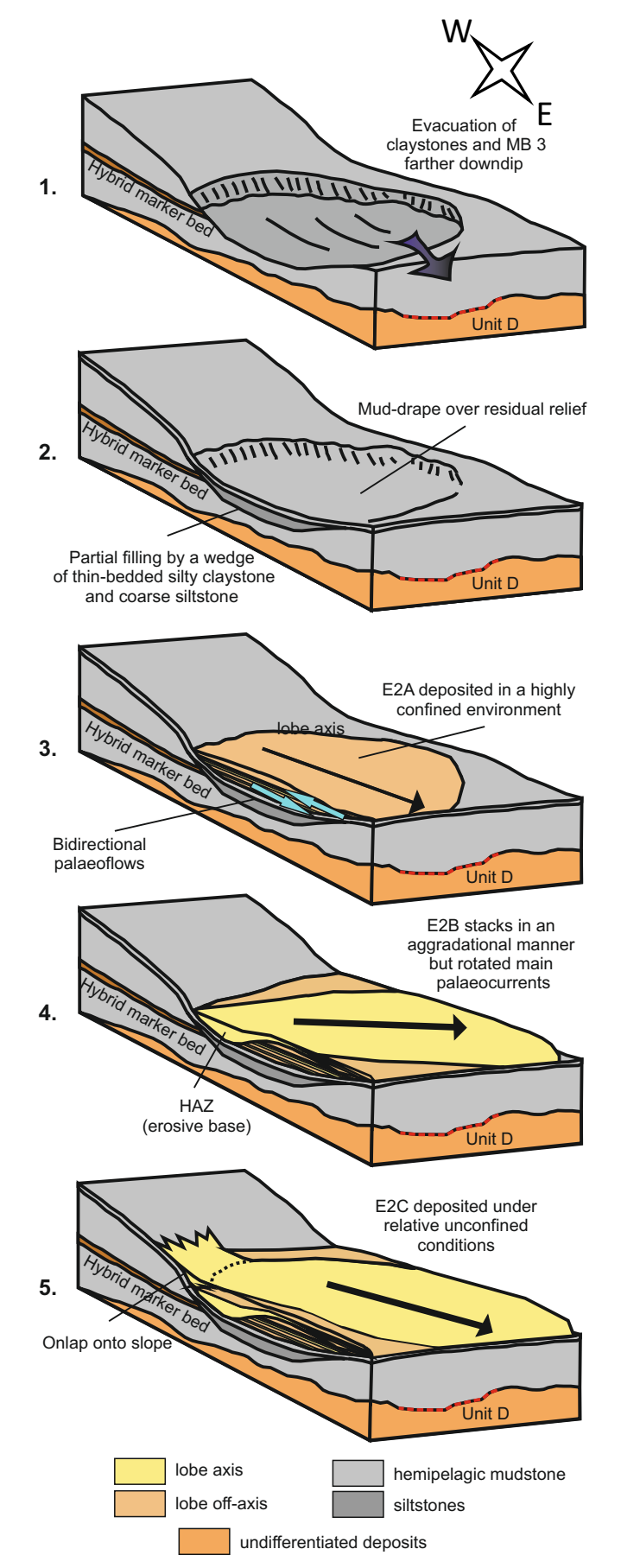
W
E
1.
Evacuation of claystones and MB 3 farther downdip
Hybrid marker bed
Unit D
2.
Mud-drape over residual relief
Hybrid marker bed
Partial filling by a wedge of thin-bedded silty claystone and coarse siltstone
Unit D
3.
E2A deposited in a highly confined environment
lobe axis
Hybrid marker bed
Bidirectional palaeoflows
Unit D
4.
E2B stacks in an aggradational manner but rotated main palaeocurrents
Hybrid marker bed
HAZ (erosive base)
Unit D
5.
E2C deposited under relative unconfined conditions
Hybrid marker bed
Onlap onto slope
Unit D
lobe axis
lobe off-axis
undifferentiated deposits
hemipelagic mudstone
siltstones

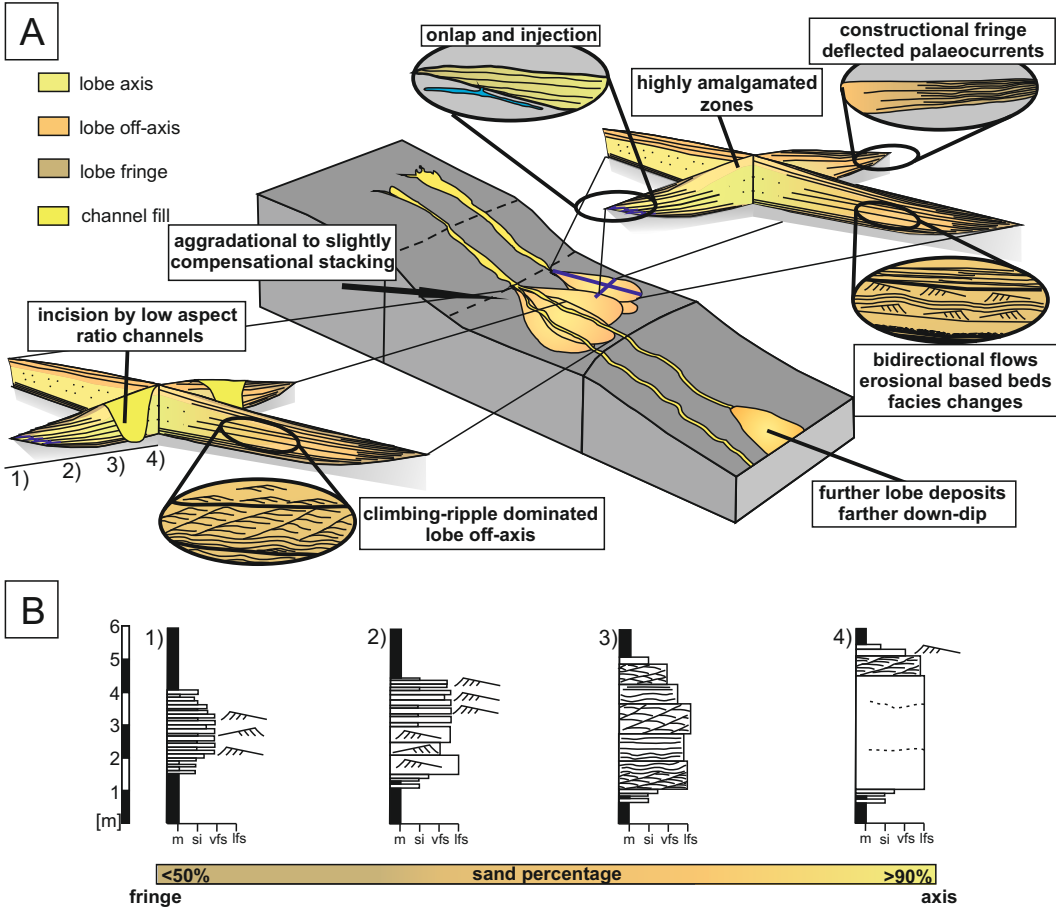
A
lobe axis
lobe off-axis
lobe fringe
channel fill
onlap and injection
constructional fringe
deflected palaeocurrents
highly amalgamated
zones
aggradational to slightly
compensational stacking
incision by low aspect
ratio channels
bidirectional flows
erosional based beds
facies changes
1)
2)
3)
4)
climbing-ripple dominated
lobe off-axis
further lobe deposits
farther down-dip
B
6
5
4
3
2
1
[m]
1)
2)
3)
4)
m si vfs lfs
<50%
sand percentage
>90%
fringe
axis